Desalination and Water Treatment
www.deswater.com

doi: 10.5004/dwt.2022.28808

271 (2022) 192–205
September

Optimized preparation of hydroxyapatite-modified carbonized rice husk and its adsorption property for Cr(VI) ions

Chenglong Zou[a,*], Kun Guan[a], Fahui Nie[a], Xiaohang Sun[b], Wenjie Liu[a]

[a]*School of Civil Engineering and Architecture, East China Jiao Tong University, 808 East Shuanggang Road, Nanchang 330013, Jiangxi, China, emails: zoujoseph@163.com (C. Zou), 2296173039@qq.com (K. Guan), 50124165@qq.com (F. Nie), 1173944503@qq.com (W. Liu)*
[b]*Ocean College, Zhejiang University, Zhoushan 316021, Zhejiang, China, email: l210127@zju.edu.cn (X. Sun)*

Received 8 January 2022; Accepted 1 August 2022

ABSTRACT

Rice husk (RH) is one of the widespread agricultural waste materials in the world. At present, most of the husks are either burned out or thrown away as waste, causing serious environmental pollution. This study prepared the hydroxyapatite-modified carbonized rice husk (HAP@CRH) nanocomposites from rice husk (RH) with modifications, aiming to explore the feasibility of preparing heavy metal ion sorbents. The preparation process affecting its adsorption properties on Cr(VI) ions was systematically investigated, which was optimized by carbonizing RH at 600°C for 2.0 h to produce CRH and then depositing hydroxyapatite particles on the surface of CRH with a Ca^{2+}/CRH ratio of 0.2 g/g. The physiochemical properties of samples were characterized. After modifications to be HAP@CRH, the surface presented a honeycomb-like structure as its porosity increased. The Brunauer–Emmett–Teller specific surface area increased from 1.06 m^2/g (RH) to 193.64 m^2/g (CRH) and 183.91 m^2/g (HAP@CRH) respectively, the total pore volume increased from almost zero to 0.089 and 0.202 cm^3/g, respectively. The results demonstrated the effective adsorption property of HAP@CRH for Cr(VI) ions as the removal rate of 98.57% and the adsorption amount of 5.91 mg/g were achieved within 24.0 h with adsorbent dosages of 5.0 g/L for initial Cr(VI) concentration of 30 mg/L at 30°C and pH 2.0. This study is expected to promote the utilization of wasted rice husk biomass and provide a new economic and feasible adsorption material for wastewater treatment so as to achieve the purpose of treating waste with waste.

Keywords: Rice husk; Hydroxyapatite; Cr(VI) ions; Adsorption; Carbonization

1. Introduction

With the increasing consumption of mineral resources on the earth, some resources have been nearly exhausted and the environmental pollution is getting worse in the meantime. As a result, researchers have turned their attention to the development and utilization of renewable resources, especially biomass [1]. In recent years, agricultural and forestry biomass resources have attracted lots of attentions in that they're of large quantity, renewable with a short renewable cycle, biodegradable, and environmentally friendly [2,3]. If agricultural and forestry waste biomass can be rationally and comprehensively utilized, it will not only ease the environmental problem but also create certain economic value.

Rice husk (RH) is one of the universal agricultural waste materials accountings for 20~22 wt.% of the rice [4,5], and about 130~140 million tons of rice husks are produced annually in the world [6]. At present, most of the rice

* Corresponding author.

husks are either burned out or thrown away as waste [7]. The former will discharge harmful gases containing toxic substances and suspended particles into the atmosphere, which will lead to heavy haze, acid rain, and other serious environmental pollution, and make people suffer serious respiratory diseases as well [8,9]. If the rice husk was used effectively, it will become a huge cheap renewable resource. At present, some researchers focus on applying it to wastewater treatment with advantages of local availability, high chemical stability, and mechanical strength [9], and it can be collected directly from the rice processing plant without collection costs like other waste biomass. However, the insufficient active functional groups and points on the surface of natural rice husk limit the adsorption property for heavy metal ions, for which the RH needs modifications to widen its application. A series of studies have shown that RH is a potential biological adsorbent with a strong ability to remove various heavy metal pollutants after chemical and physical modifications [10,11].

Hydroxyapatite (HAP, $Ca_{10}(PO_4)_6(OH)_2$) is a calcium hydrogen phosphate compound with a chemical composition and structure similar to that of mammalian bones [12]. It possesses good ions adsorption and exchange characteristics as the Ca^{2+} and OH^- on HAP can be exchanged by other ions due to its special hexagonal crystal structure [13]. And the metal ions in wastewater can be successfully immobilized through interaction with the reaction sites (e.g., –CaOH, –POH, $–CaOH^{2+}$, and $–PO_3H^-$) on the surface of HAP to form composite phosphate [14,15]. As a kind of environmental protection material, HAP-containing adsorbents can be safely used to remove the pollutants in water [16]. However, HAP nanoparticles tend to aggregate into larger particles (micrometers to millimeters range) in aqueous solutions because of the high surface energy caused by van der Waals forces, thereby reducing aqueous dispersibility and inhibiting chemical reactivity [17,18] and ultimately resulting in the weakening of its adsorption property of contaminants. If the HAP nanoparticles were loaded onto the rice husk, the reunion problem will be solved and desirable adsorption properties will be produced. Moreover, the adsorption capacity of the synthetic adsorbent to pollutants will be improved.

The rapid stride in industrialization brought about a major concern [19] and at present toxic chemical agents discharged into water bodies from industries are a severe threat to the survival of living organisms as well as the ecological balance [20]. The anthropogenic discharge of toxic agents containing heavy metal ions used in household products, industries, agriculture, and industrial effluents are the major sources of environmental contamination [21]. Heavy metal ions pollution has become an urgent problem to be solved all over the world. Various methods have been applied to treat wastewater containing heavy metal ions pollution. Each of these methods has advantages and disadvantages, which in most cases due to spending of the high cost and time are not economical [22]. The adsorption process is one of the well-established and powerful techniques to remove heavy metal ions from wastewater [23]. Compared with traditional adsorbents, biosorption has more advantages. It is cost-effective and environmentally friendly as a variety of adsorbents are available naturally and these adsorbents can be modified to enhance their adsorption properties of any type of pollutant [24].

The purpose of this study is to explore the feasibility of preparing heavy metal ion adsorbents from RH biomass with modifications and explore the modification methods for better adsorption properties. RH was firstly modified into carbonized rice husk (CRH), and then HAP nanoparticles were deposited onto the surface of CRH via the hydrothermal method to prepare hydroxyapatite-modified carbonized rice husk (HAP@CRH) composites. The conditions of the preparation process (carbonization temperature, carbonization time, and loading amount of HAP) were assumed as factors affecting the adsorption property of the product HAP@CRH and which were optimized to improve the adsorption property. The physiochemical properties including textural properties, surface morphology, specific surface area, surface functional groups, and the electrical changes of the HAP@CRH were characterized by Fourier-transform infrared spectroscopy (FT-IR), X-ray diffraction (XRD), surface area, pore structure analysis, and scanning electron microscopy (SEM) and zeta potential measurements. In the meantime, the adsorption properties on Cr(VI) ions affected by the preparation process were systematically investigated with batch adsorption experiments. The study is expected to promote the utilization of wasted rice husk biomass and provide a new economic and feasible adsorption material for the treatment of wastewater with heavy metal ions, so as to achieve the purpose of treating waste with waste. It is of great significance for the wider application of discarded rice husks in environmental protection and the improvement of its resource utilization value.

2. Experimental

2.1. Materials and chemical reagents

Rice husks (RH) were obtained from a Rice Milling Plant in Yichun City (Jiangxi Province, China). The rice husks were crushed and sieved to particle sizes of 0.3~0.5 mm, and then they were physically purified with distilled water (DI) to remove dust impurities and dried at 105°C for 12 h before they were stored for subsequent use.

The chemical reagents of analytical grade were purchased from Xilong Technology Co., Ltd., (China), including phosphoric acid (H_3PO_4, 85.1%), hydrochloric acid (HCl, 37.0%), sodium hydroxide (NaOH, 99.7%), calcium chloride ($CaCl_2$, 96.0%), diammonium hydrogen phosphate ($(NH_4)_2HPO_4$, 99.0%), ammonia ($NH_3{\cdot}H_2O$, 26.0%), and potassium dichromate ($K_2Cr_2O_7$, 99.0%).

2.2. Preparation of hydroxyapatite-modified carbonized rice husk

There are two stages for the synthesis of the hydroxyapatite-modified carbonized rice husk (HAP@CRH) [25]. The first stage is to obtain carbonized rice husk (CRH) through a typical slow pyrolysis process [26]. The second stage is to deposit HAP particles onto the surfaces of CRH with different Ca^{2+}/CRH ratios to prepare hydroxyapatite-modified carbonized rice husk (HAP@CRH) through the co-precipitation method proposed in a previously published article [26,27]. The preparation procedures of

HAP@CRH are shown in Supplementary Fig. S1 schematic representation and described as follows:

Firstly, approximately 50 g of RH which had been rinsed with DI water and dried at 105°C was activated in 750 mL of H_3PO_4 solution (150 g/L) at 50°C for 24 h. Then the samples were carbonized in a programmable box muffle furnace at various temperatures for a certain time in N_2 atmosphere (15 mL/min) with a heating rate of 10°C/min. After carbonization, the samples were cooled down in the presence of N_2 flow. CRH was obtained after the samples were cleaned thoroughly with HCl solution (100 g/L) and deionized water, and dried at 105°C for 24 h.

Secondly, an amount of CRH was added to $CaCl_2$ solution (1 mol/L) and mixed adequately to produce a suspension solution, the pH of which was adjusted to 10 with ammonium hydroxide ($NH_3{\cdot}H_2O$). The same volume of $(NH_4)_2HPO_4$ solution (0.6 mol/L) was added dropwise into the suspension solution with a peristaltic pump under vigorous stirring. The pH of the solution was adjusted to 10 with ammonium hydroxide ($NH_3{\cdot}H_2O$), and then the mixed suspension solution was stirred fiercely at 45°C for 1.0 h and left to age for 48 h at 25°C. Finally, the precipitate was isolated by centrifugation and washed with DI water, followed by a drying process at 80°C. Afterward, the HAP@CRH was obtained, and it was stored for subsequent use after sieving to pass through 80 meshes.

2.3. Characterization methods

The thermogravimetric analysis/derivative thermogravimetry (TG/DTG) analysis of the raw RH was conducted through a thermal analyzer (NETZSCH STA F5 Jupiter, Germany) under the N_2 atmosphere with the temperature range of room temperature to 800°C (10°C/min). The infrared spectra of the samples were recorded by means of the FT-IR spectrometer (Nicolet iS10 FT-IR, Thermo Nicolet Corporation, USA) over wavenumbers of 400–4,000 cm^{-1}. The XRD patterns of samples were recorded via X-ray diffraction (XRD, Bruker D8 Advance, Germany) with Cu Kα radiation (λ = 1.5406 Å) over a diffraction angle (2θ) range of 10°–80° with a scan speed of 4°/min at 40 kV and 20 mA. The surface morphologies of the samples were observed by taking SEM images with the assistance of scanning electron microscopy (SEM, SU8020 SEM Systems, Hitachi, Japan). The surface characteristics of the samples were demonstrated through a surface area and porosimetry analyzer (V-Sorb 2800, Gold APP Instruments Corporation, China), while the N_2 vapor adsorption–desorption isotherms were recorded at 77 K following degasification at 150°C for 6 h. The specific surface area, pore-size distributions, micropore volume, micropore surface area, and total pore volumes were calculated by analyzing the isotherm through the corresponding method. The zeta potential of samples at different pH was measured with a zeta potential analyzer (Zetasizer Nano ZS90, Thermo Fisher, USA).

2.4. Batch adsorption experiments

All adsorption experiments were done in batches in a thermostatic water bath oscillator at 170 rpm and 30°C. A predetermined amount of $K_2Cr_2O_7$ was added into deionized water to obtain the Cr(VI) ions simulated wastewater with a certain concentration in the presence of hydrochloric acid.

In each experiment, 200 mL of test solution was added into a 500 mL conical flask, and then its pH was adjusted to 2.0 by using 0.01 M HCl or 0.01 M NaOH solutions. The flask was shaken in an electricity-driven thermostatic water bath oscillator, and then 1.0 g of absorbent samples were added to the solution. Mixed samples were taken at intervals over the adsorption reaction, and then immediately filtered through a 0.22 μm PTFE membrane syringe filter. The concentrations of residual Cr(VI) ions in the filtrate were determined by an AAS novAA 400 hydrogen flame atomic absorption spectrometer (Analytik Jena AG, Germany). All experiments were conducted 3 times to examine their reproducibility and to calculate their mean value.

2.5. Data processing

The adsorption removal rate (R, %) of Cr(VI) ions is calculated by using Eq. (1):

$$R = \frac{C_0 - C_e}{C_0} \times 100 \quad (1)$$

where C_0 and C_e are the initial concentration of Cr(VI) ions and the Cr(VI) ions concentration at equilibrium (mg/L) respectively.

3. Results and discussion

3.1. Characterizations of materials

3.1.1. TG-DTG analysis

The decomposition of RH heated at 300°C~800°C for CRH biochar preparation was evaluated by TG-DTG analysis, illustrating the evolution of non-condensable gases and residual solid components (i.e., biochar) [28]. The TG-DTG curves are displayed in Fig. 1.

As shown in Fig. 1, the weight loss of RH occurs over a wide range of temperatures, especially at 180°C~500°C. Three obvious peaks of weight loss could be seen in the DTG curve. The peak at 81.6°C is a result of the drying and evaporation of light contents such as free water [29]. The decomposition peaks at 278.5°C and 337.1°C are attributed to the decompositions of hemicelluloses and cellulose respectively [30], which are close to the values reported for pure hemicelluloses (268°C) and cellulose (355°C) [31]. Thus, the partial cellulose components of samples were thermally changed at 300°C~500°C. Whereas all the raw biopolymers, hemicelluloses, and cellulose of samples that were processed under the temperature over 500°C were completely decomposed.

3.1.2. Specific surface area and pore structure analysis

The conditions of the preparation process play crucial roles in governing the physical and chemical properties of biochar [32]. The effect of the preparation process on the physical and chemical structure was investigated through characterization analysis, which provides evidence for its

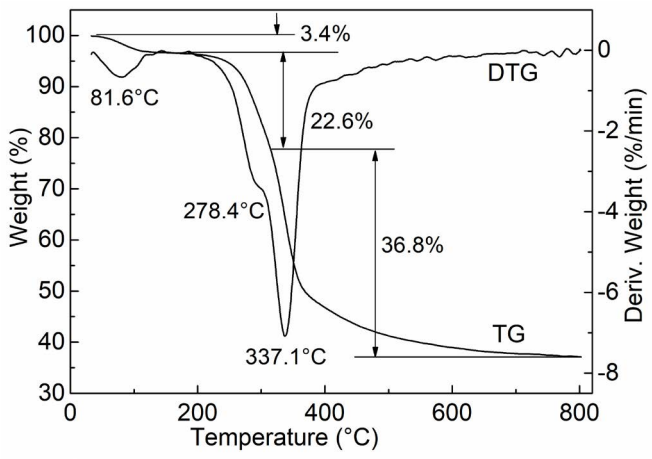

Fig. 1. TG-DTG curves of rice husk.

Table 1
Specific surface area and pore structure parameters of rice husk (RH), carbonized rice husk (CRH), and hydroxyapatite-modified carbonized rice husk (HAP@CRH) samples

Samples	RH	CRH	HAP@CRH
BET surface area (m^2/g)	1.06	193.64	183.91
Langmuir surface area (m^2/g)	1.52	257.63	246.24
Microporous surface area (m^2/g)	0.06	113.45	83.81
Total pore volume (cm^3/g)	0.008	0.089	0.202
Micropore volume (cm^3/g)	0.000	0.053	0.039
Average pore-size (nm)	27.97	2.40	15.14
Average mesopore size (nm)	25.43	6.36	5.64

effect on the adsorption property of the material. The specific surface area and pore structure analysis can reflect the influence of preparation conditions on the physical structure of materials through specific test data. Therefore, the specific surface area and pore structure of the modified material under different conditions were analyzed in detail. Supplementary Fig. S2 serves as good examples to show the N_2 adsorption–desorption isotherm and pore-size distribution curves of RH, CRH prepared by carbonization at 600°C for 2.0 h, and HAP@CRH prepared with a Ca^{2+}/CRH ratio of 0.2 g/g. And Table 1 illustrates the specific surface area, pore volumes, and average pore-size of those samples, while the specific surface area of raw RH, CRH, and HAP@CRH prepared under different conditions are shown in Fig. 2.

According to supplementary Fig. S2, the N_2 adsorption–desorption isotherms of the RH belong to a type-II with a H_3 type hysteresis loop, indicating the mesoporous structure of the adsorbents. It presents typical type-IV sorption isotherms with type H_3 hysteresis loops in samples CRH and HAP@CRH. Large hysteresis areas in the isotherms were clearly observed for all samples, suggesting a wide distribution of pore-size [33]. The pore structure analysis also reveals that the material has a wide pore diameter distribution. Compared with RH, the isotherm of the CRH sample steepened at low P/P_0, indicating that the volume of micropores and mesopores increased [34]. However, the isotherm of the HAP@CRH sample steepened over the range of P/P_0 of 0.80–0.99, which meant that the volume of macropore increased. The results are consistent with Table 1.

As can be seen in Table 1, the Brunauer–Emmett–Teller (BET) and Langmuir specific surface area increased from 1.06 m^2/g and 1.52 m^2/g to 193.64 m^2/g and 257.63 m^2/g respectively after carbonizing RH to CRH. In particular, the micropore area increased from almost zero to 113.45 m^2/g. While RH was carbonized to CRH, there was a significant decrease in the average pore-size and average mesopore size, especially the micropore area and volume. This was because the organic components in the raw rice husk decomposed into volatile gas under the condition of high temperature and no oxygen, and then the remaining carbon atoms crossed link to form amorphous sheets of carbon, resulting in the appearance of a large number of pores with different diameters on the surface and inside of the carbon. The specific surface area and pore area were slightly reduced after further modification to produce HAP@CRH, while the total pore volume increased from 0.089 to 0.202 cm^3/g. The reason for such phenomenon might be that the hydroxyapatite synthesized with larger pore diameters and a smaller specific surface area as well as the original pore channels of CRH were covered with hydroxyapatite.

The adsorption occurs mainly on the internal and external surfaces of adsorbents. Hence, the specific surface area and pore structure of adsorbents are important factors affecting the adsorption properties [26]. As shown in Fig. 2, the specific surface area of the CRH was affected by the carbonization temperature and time of the preparation process, while the specific surface of the HAP@CRH was affected by the ratio of Ca^{2+} to CRH. This is probably due to that under low carbonization temperature, the tar produced will cause internal blockage and incomplete volatilization which leads to the formation of a large number of micropores in the material. With the increase of temperature, the micropores increase or collapse to form large pores, giving rise to a sharp increase in the specific surface area. If the pyrolysis treatment time is too long, the pore structure will be sintered and result in poor pore structure [35]. As the specific surface area of hydroxyapatite is relatively small, the specific surface area of the HAP@CRH decreases gradually with the load amount of HAP increasing.

3.1.3. Scanning electron microscope analysis

The surface morphology of rice husk samples at different modification stages has been observed via SEM. The SEM microphotographs of RH, CRH prepared at 600°C for 2.0 h, and HAP@CRH prepared with a Ca^{2+}/CRH ratio of 0.2 g/g are provided below as examples in Fig. 3.

Judging from the changes of surface texture shown in SEM micrographs, the developments of surface morphology and pore structure have been significantly affected by the treatments. The images of the untreated raw rice husk present a fairly smooth structure with little pore structure. Whereas images of the CRH show its surface became rougher with small pores and small fragments of irregular shapes, and the cracks on the surface of the CRH samples were caused by the pyrolysis of organic matter.

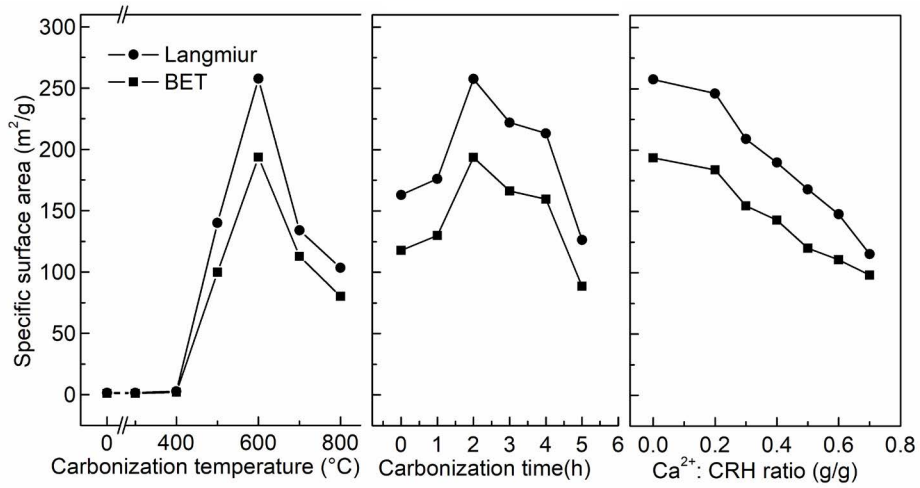

Fig. 2. Effect of preparation process parameters on the Langmuir and BET specific surface area of carbonized rice husk and hydroxyapatite-modified carbonized rice husk samples.

After further synthesis of HAP@CRH, a honeycomb-like structure appeared as the surface porosity increased. The results of SEM analysis are consistent with the data of the specific surface area and pore structure analysis.

3.1.4. FT-IR analysis

The adsorption properties of an adsorbent can be enhanced by modifying the structure and surface chemistry [36]. FT-IR was used to analyze the chemical structure of the samples affected by the modification process by checking the major differences in the chemical groups. The infrared spectra of the samples RH, CRH, and HAP@CRH are shown in Fig. 4.

The infrared spectrogram demonstrates that the structure and characteristics of functional groups of each material changed obviously after modification in its previous stage. The peaks at 3,435 and 1,638 cm^{-1} shown in all samples due to the stretching and bending vibration of the hydroxyl group (O–H) in adsorbed water by the material [37]. The peak at 798 cm^{-1} was connected with the stretching vibrations of Si–O groups [38], and the peak at 467 cm^{-1} was caused by the bending vibration of the Si–O–Si group, which were typically observed in the three samples with the presence of silica in RH [39]. The peak near at 1,097 cm^{-1} corresponded to the Si–O–Si stretching vibration of silica [38], while it was covered in HAP@CRH by other peaks.

There are abundant peaks in the RH samples. The peak at 1,638 cm^{-1} may belong to the carbonyl group or quinone [40]. The peak at 2,923 cm^{-1} was a result of the antisymmetric stretching vibration of C–H bond in methylene ($-CH_2$); the peak at 1,510 cm^{-1} was due to the vibrates of the amido group of plant proteins; the peak at 1,457 cm^{-1} was attributed to the skeletal vibration of C=C; the peak at 1,420 cm^{-1} was related to the stretching vibration of C–N; the peak at 1,378 cm^{-1} was owing to the bending vibration of C–H; the peak at 1,162 cm^{-1} belonged to the asymmetric vibration of C–O–C; the peak at 1,158 cm^{-1} resulted from the bending vibration of a single bond C–OH; and the peak at 899 cm^{-1} was caused by the rocking vibration of $-CH_2$ [41,42]. After the carbonization of RH, these absorption peaks disappeared and the absorption strength of CRH weakened at the peak of 1,638 cm^{-1}, which was possible because the organic materials such as cellulose and polysaccharides contained in rice husks were broken down in the process of dehydrogenation, deoxidation, and dihydroxylation [43]. The vibration peak at 669 cm^{-1} appeared due to the bending vibration of the carboxyl group which was observed in all three samples. The intense peaks at 1,092 and 1,035 cm^{-1} corresponded to the asymmetrical stretching vibration of the phosphate (PO_4^{3-}) groups in the crystal lattice of HAP, and the peaks at 633, 602, and 565 cm^{-1} were relevant to asymmetric bending vibration of phosphate (PO_4^{3-}) groups [44,45]. Meanwhile, the peak at 962 cm^{-1} was attributed to the symmetric stretching mode of the PO_4^{3-} ions [46]. The small peak at 878 cm^{-1} detected was due to the presence of HPO_4^{2-} [15]. The above data indicate that hydroxyapatite was successfully synthesized and loaded on the carbonized rice husk.

3.1.5. XRD analysis

The crystal phases of the main compositions of the three samples were analyzed via XRD [47]. As the results shown in Fig. 5, the diffraction peaks of CRH and HAP@CRH samples changed obviously after modification, suggesting that the structure of the main composition of the two samples changed significantly.

The diffraction peaks at 2θ = 15.32°, 22.31°, and 34.52° observed in RH samples are ascribed to the cellulose [43]. There should have been a characteristic peak around 22° as an amount of silica (SiO_2) in the rice husk, yet it was concealed [48]. The obvious broad reflection band between 22° and 25° was the overlapping peak of the diffraction peaks of carbon (002) crystal surface and silica (SiO_2) in rice husk [46]. The peak demonstrated a wide range of deformation and presented as a dispersion peak (amorphous carbon), which was due to the increase of carbon disorder degree (low degree of crystallization) with the thermal degradation of organic matter in rice husk [49]. The other weak

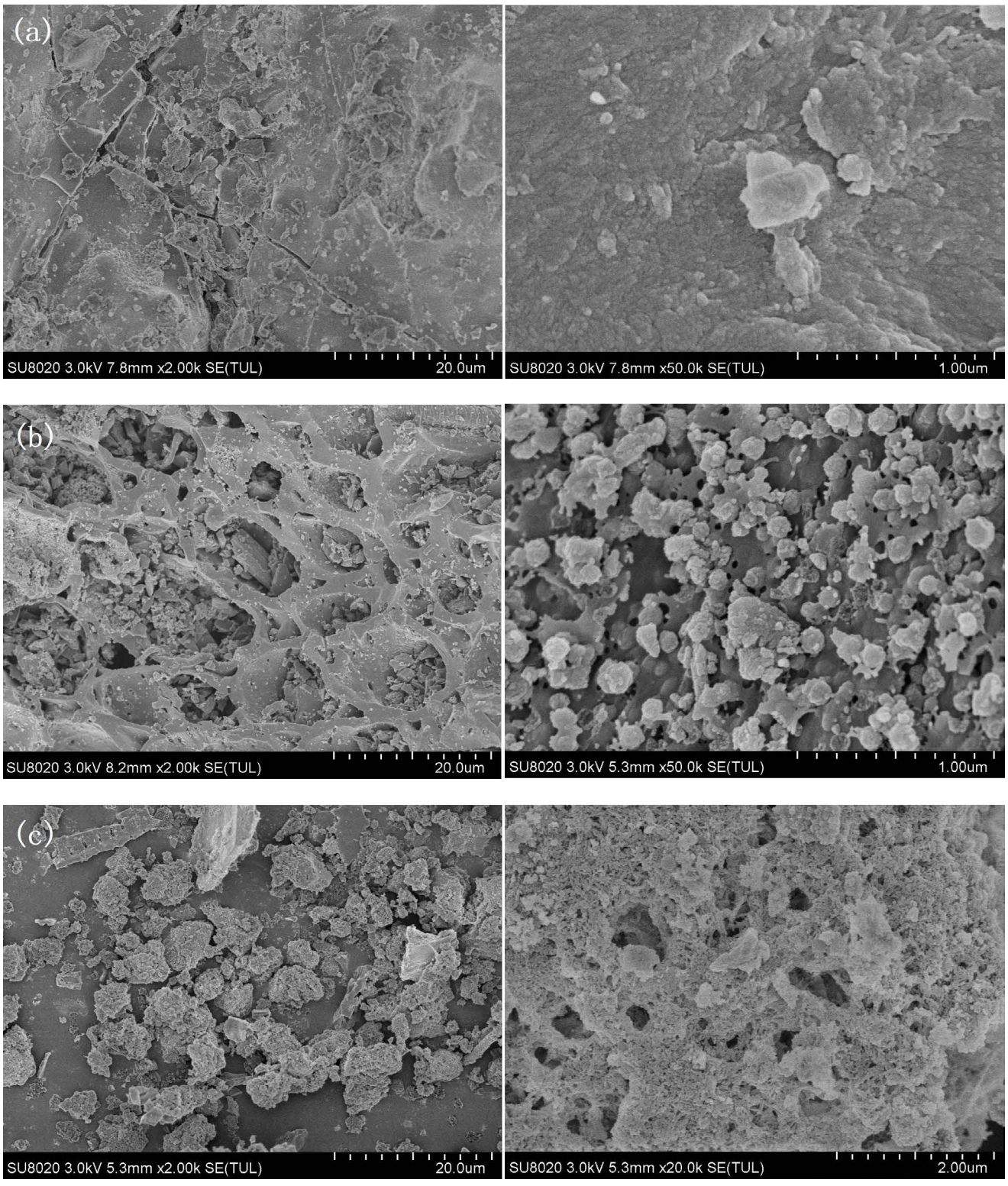

Fig. 3. SEM images of (a) rice husk, (b) carbonized rice husk, and (c) hydroxyapatite-modified carbonized rice husk samples.

band (not obvious in the figure) reflected at 44.52° was correspondent to the (100) plane of carbon (JCPDS: 00-011-0646), which indicated the formation of a turbostratic structure of amorphous carbon [50]. According to the XRD patterns in Fig. 5, the HAP@CRH presented diffraction characteristic peaks at 22.94°, 25.88°, 28.28°, 29.08°, 31.77°, 32.19°, 32.98°, 34.06°, 39.86°, 42.44°, 43.80°, 46.89°, 48.31°, 49.47°, 53.14° and 64.26°, which were attributed to the (111),

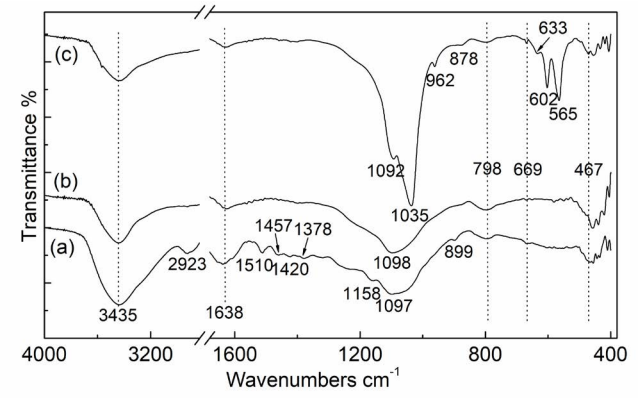

Fig. 4. FT-IR spectra of (a) rice husk, (b) carbonized rice husk, and (c) hydroxyapatite-modified carbonized rice husk samples.

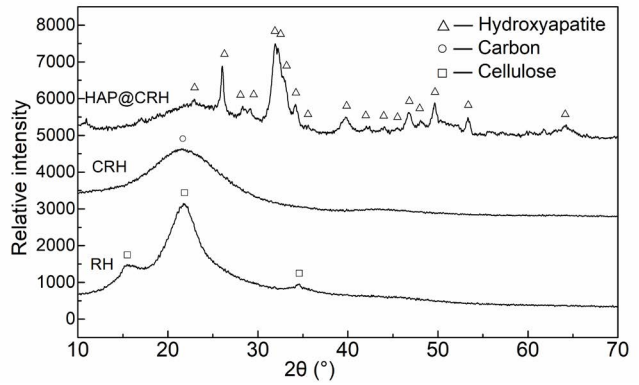

Fig. 5. XRD patterns of (a) rice husk, (b) carbonized rice husk, and (c) hydroxyapatite-modified carbonized rice husk samples.

(002), (102), (201), (211), (112), (202), (130), (302), (113), (222), (132), (213), (004) and (323) planes of hydroxyapatite (HAP) crystal respectively (JCPDS No. 09-0432) [51]. XRD analysis reveals that the HAP was successfully synthesized and loaded onto the CRH, which was consistent with the results of FT-IR analysis.

3.1.6. Zeta potential

The potential on the surface of the adsorbent reflects the ability of materials to remove anionic, cationic, or molecular pollutants, which is an important parameter affecting adsorption applications [52]. In this study, the potential changes on the HAP@CRH surface relative to CRH were investigated through zeta potential analysis as references for adsorption property studies of HAP@CRH. Zeta potentials of CRH and HAP@CRH at various pH are displayed in Fig. 6.

As shown in Fig. 6, the potentials decreased with the increase of pH, and the zero charge points (PZC) of CRH and HAP@CRH were determined to pH 2.9 and pH 3.7, respectively. The zeta potential of HAP@CRH was higher than that of CRH at pH 2.0–4.5 and was slightly lower than that of CRH at pH 4.5–10.0. As pH increased from pH_{PZC} to 10.0, the functional groups of HAP@CRH underwent deprotonation, resulting in a decrease from 0 to –27.8 mV

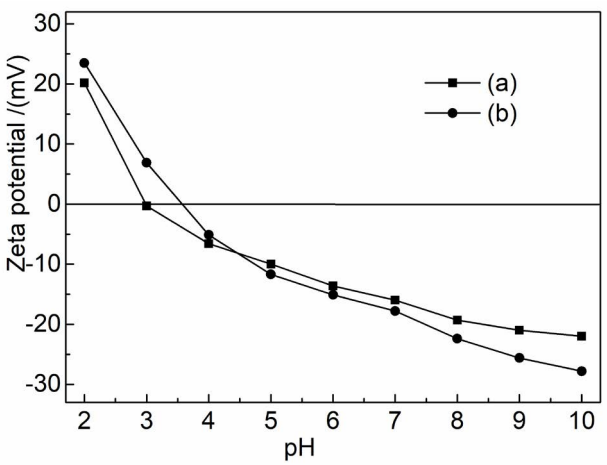

Fig. 6. Zeta potentials of (a) carbonized rice husk and (b) hydroxyapatite-modified carbonized rice husk in the pH range of 2–10.

of its zeta potential. The negative charges could cause oxygenated functional groups of basic characteristics such as lactone or hydroxyl groups to be chemisorbed at the surface of the pores [53].

It will lead to a high affinity with positive species on the HAP@CRH composite adsorbent over the wide pH range (3.7–10.0) [54]. Whereas, the Cr(VI) ions exist in the different forms of $HCrO_4^-$, $Cr_3O_{10}^{2-}$, $Cr_4O_{13}^{2-}$, and $Cr_2O_7^{2-}$ in an acidic environment [55]. Hence, the adsorption capacity of HAP@CRH to Cr(VI) ions might be increased owing to the electrostatic attraction between Cr(VI) ions and the positively charged surface at low pH.

3.2. Adsorption properties

The adsorption actions of heavy metal ions on materials can be classified into physical adsorption, chemical adsorption, and ion exchange adsorption [56]. The physical adsorption is mainly affected by the specific surface area and pore structure of the adsorbent, chemical adsorption is mainly affected by the types and numbers of functional groups on the surface, and ion exchange adsorption is mainly affected by the number and balance of exchangeable ions on the surface of the adsorbent. The characterization results indicate that the preparation process has a great influence on the material structure during the process of processing RH into HAP@CRH, which will also seriously affect the adsorption property of the material. Therefore, the preparation process has been optimized after comparing the effects of various modification parameters on the adsorption efficiency of Cr(VI) ions. Meanwhile, the adsorption mechanism was explored by analyzing the influence of the changes of the physical and chemical structure on the adsorption properties of the products.

3.2.1. Effect of carbonization temperature of CRH

The surface structure is a crucial factor determining the adsorption property as the adsorption reaction occurs mainly at the surface of solid adsorbents [57]. However,

the characterizations showed that the carbonization temperature is a significant factor affecting the morphology of CRH. Hence, adsorption experiments had been conducted to explore the adsorption property of adsorbent to Cr(VI) ions affected by the carbonization temperature. The experiments were conducted as follows: the Cr(VI) ions solution with an initial concentration of 30 mg/L was treated with CRH (carbonizing time of 2.0 h) dosages of 5.0 g/L at 30°C, pH = 2.0, within a contact time of 24 h. Fig. 7 shows the carbonization temperature affecting both the removal rate (R) and residual concentration (C_e) of Cr(VI) ions.

In Fig. 7, the adsorption effect of CRH on Cr(VI) ions increased with the carbonization temperature increasing from 300°C to 600°C, while the adsorption effect decreased when the temperature exceeded 600°C. There are several reasons accounting for this phenomenon: first, the organic components in biomass raw materials decomposed and volatilized under high temperature and oxygen limit; second, large numbers of pores with different diameters appeared on the surface and inside of the remaining solid components, providing lots of adsorption sites for Cr(VI) ions. In addition, raw biopolymers hemicelluloses and cellulose of samples were decomposed to form new organic functional groups which then chelated with Cr(VI) ions. When the carbonization temperature is too high, some functional groups will be destroyed so that the adsorption of metal ions will be reduced [58]. Meanwhile, the surface structure collapsed and the holes will be blocked, hindering the transport and diffusion of heavy metal particles. This coheres with the specific surface area and pore structure analysis mentioned above. Based on the adsorption experiment effect and analysis, the carbonization temperature is optimized to 600°C.

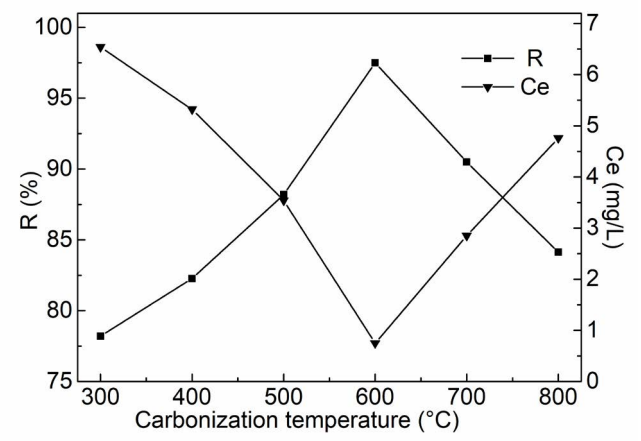

Fig. 7. Effect of carbonization temperature on the adsorption removal rate (R) and residual concentration (C_e) of Cr(VI) ions adsorbed by carbonized rice husk (Cr(VI) ions solution with an initial concentration of 30 mg/L treated with CRH dosages of 5.0 g/L at 30°C, pH = 2.0, within a contact time of 24 h, respectively).

3.2.2. Effect of carbonization time of CRH

The carbonization time was verified to have a great influence on the structure of the material according to characterizations, and the influence on the adsorption property of the products has been further explored through adsorption experiments. The experiments were conducted as follows: the Cr(VI) ions solution with an initial concentration of 30 mg/L was treated with CRH (carbonizing at 600°C) dosages of 5.0 g/L at 30°C, pH = 2.0, within a contact time of 24 h. The carbonization time affects both the removal rate (R) and residual concentration (C_e) of Cr(VI) ions is shown in Fig. 8.

As can be seen in Fig. 8, the CRH prepared for 2.0 h presents the best adsorption performance to Cr(VI) ions, while a short or prolonged preparation time would weaken the adsorption performance. This may be because the organic components have not completely evaporated to form the pore structure when the carbonization process conducted in high-temperature conditions doesn't last long enough. However, if the carbonization pyrolysis time is too long, the pore structure originally generated will be sintered and result in poor pore structure [55]. All of those lead to a decrease in the specific surface area and further reduce the adsorption sites, then affecting the adsorption efficiency. On the basis of the adsorption experiment effect and analysis, the carbonization time is optimized to 2.0 h.

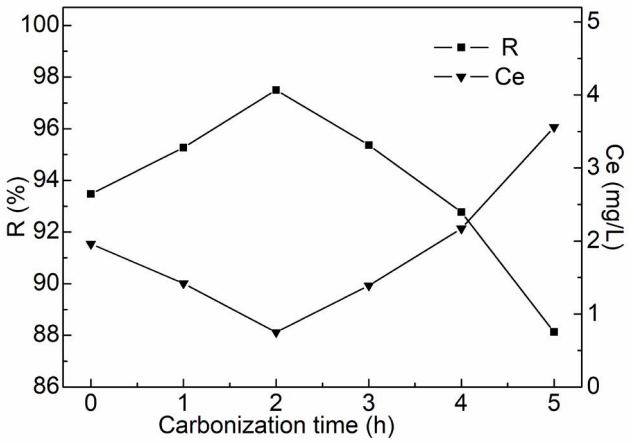

Fig. 8. Effect of carbonization time on the adsorption removal rate (R) and residual concentration (C_e) of Cr(VI) ions adsorbed by carbonized rice husk (Cr(VI) ions solution with an initial concentration of 30 mg/L treated with CRH dosages of 5.0 g/L at 30°C, pH = 2.0, within a contact time of 24 h, respectively).

3.2.3. Effect of loading amount of HPA

HAP with a large specific surface area and high microporosity can offer more interactive sites for the reaction and has special effects on heavy metal ions such as adsorption, ion exchange, precipitation, and surface complexation [59]. The purpose of the modification is to increase adsorption sites and active functional groups of CRH so as to expand its application potential in the adsorption of heavy metal ions by depositing HAP on it. However, if the load is too much, the holes in the carbonized rice husk will be blocked, the comparative area will be reduced, which then leads to a decrease of the effective adsorption sites. Therefore, the reasonable load amount of HAP on CRH (ratio of Ca^{2+} to CRH, CRH carbonized at 600°C for 2.0 h) was further

optimized based on the preparation process optimization of rice husk biochar. It was carried out by exploring the effect of HAP load on the adsorption performance of products through adsorption experiments with HAP@CRH prepared at different Ca^{2+}/CRH ratios as the experimental subject. It was conducted as follows: the Cr(VI) ions with an initial concentration of 30 mg/L were treated with an adsorbent dosage of 5.0 g/L at 30°C, pH = 2.0, within a contact time of 24 h. The effects of the Ca^{2+}/CRH ratio on both the removal rate (R) and residual concentration (C_e) of Cr(VI) ions are shown in Fig. 9.

As shown in Fig. 9, the removal rate of Cr(VI) ions increased and the residual ions concentration decreased after hydroxyapatite loading. However, the results also reveal that the adsorption removal effect gradually decreased with the increase of the HAP loading amount. This is because of although the ion exchange capacity increased with HAP loading, the original pores and surface of rice husk carbon were blocked and covered. Excessive HAP loading reduced the adsorption efficiency of HAP@CRH on Cr(VI) ions as a whole. Therefore, the preparation parameters of HAP@CRH with the best adsorption effect on Cr(VI) ions were optimized to a Ca^{2+}/CRH ratio of 0.2 g/g.

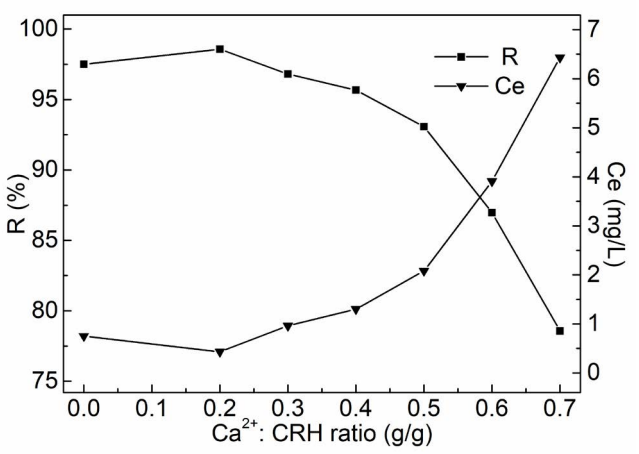

Fig. 9. Effect of Ca^{2+}/CRH ration on the adsorption removal rate (R) and residual concentration (C_e) of Cr(VI) ions adsorbed by hydroxyapatite-modified carbonized rice husk (Cr(VI) ions with an initial concentration of 30 mg/L treated with an adsorbent dosage of 5.0 g/L at 30°C, pH = 2.0, within a contact time of 24 h, respectively).

3.2.4. Comparison of adsorption properties of the three materials

On the basis of the investigation into the changes of the physical and chemical structure of the material at each modification step affecting the adsorption properties of Cr(VI) ions, the adsorption property of RH, CRH, and HAP&CRH was further compared through adsorption experiments. The experiments were conducted as follows: the Cr(VI) ions with initial concentrations range of 10–70 mg/L were treated with adsorbent dosages of 5.0 g/L at 30°C, pH = 2.0, within a contact time of 24 h. The effects of the adsorbent type on both the removal rate (R) and residual concentration (C_e) of Cr(VI) ions are shown in Fig. 10.

As is indicated in Fig. 10, the removal efficiency of adsorption Cr(VI) ions with HAP@CRH was higher than that of CRH, while both were significantly higher than that of RH. It suggests that the adsorption property has been improved after modifications. The adsorption performance of Cr(VI) by HAP@CRH was also compared with other modified rice husk materials, and the result was listed in supplementary Table S1. The comparison results indicated that the HAP@CRH material obtained with these modifications shows better adsorption capacity for Cr(VI) ion. The contributing factors are as follows: as shown in Table 1, the specific surface area and the total pore volume of HAP@CRH and CRH were increased after modification, producing more adsorption sites on the surface [57]. The increase of the pore-size of CRH was beneficial for the diffusion of Cr(VI) ions into pores, promoting the utilization of adsorption sites on the pore surface significantly. SEM results also showed that the surface of HAP@CRH and CRH were rough with rich pores. The Cr(VI) ions exist in the forms of $HCrO_4^-$, $Cr_3O_{10}^{2-}$, $Cr_4O_{13}^{2-}$, and $Cr_2O_7^{2-}$ in acidic environments [58]. The zeta potential of HAP@CRH was higher than that of CRH at pH 2.0, indicating there were more positively charged metal-binding sites and showing

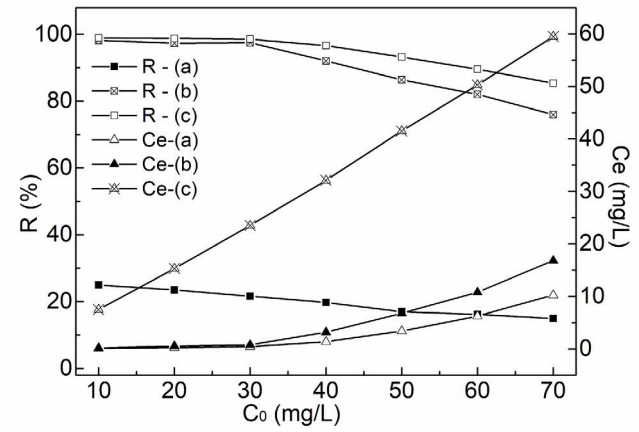

Fig. 10. the removal rate (R) and residual concentration (C_e) of Cr(VI) ions adsorbed by (a) rice husk, (b) carbonized rice husk, and (c) hydroxyapatite-modified carbonized rice husk samples (Cr(VI) ions with initial concentrations range of 10–70 mg/L treated with adsorbent dosages of 5.0 g/L at 30°C, pH = 2.0, within a contact time of 24 h, respectively).

stronger electrostatic attraction and/or by the binding of Cr(VI) in the anions form with acidic functional groups. Moreover, the number of protons available on the surface of the HAP@CRH increased and resultantly, promoting attraction between Cr(VI) in the anions form and the adsorbent whose adsorption capacity has been enhanced [60]. The Cr(VI) ions in solution were exchanged with lots of hydroxide and phosphate ions on the surface of HAP@CRH in the adsorption process, and they could be successfully immobilized through interaction with the reaction sites (e.g., –CaOH, –POH, $–CaOH^{2+}$ and $–PO_3H^-$) on the surface of HAP to form composite phosphate [61]. Thus, the adsorption effect of CRH on heavy metal ions

can be improved after it was modified to be HAP@CRH. In addition, the FT-IR study clearly delineates the functional groups such as $–NH_2$, –COOH, and –OH on the surface of the adsorbent, which will interact with Cr(VI) ions to promote the adsorption of Cr(VI) process [62].

4. Conclusion

The hydroxyapatite-modified carbonized rice husk was prepared in this study and the preparation process was optimized based on characterization analysis and adsorption experiments. Meanwhile, this study found that to obtain HAP@CRH with effective adsorption performance, the raw rice husk should be carbonized and pyrolyzed for 2.0 h at 600°C to produce CRH, and then hydroxyapatite particles should be deposited on the surface of CRH with a Ca^{2+}/CRH ratio of 0.2 g/g.

With the pyrolysis of organic matter during carbonization, the surface became rougher with small pores and small fragments of irregular shapes, and cracks were created on the surface of the carbonized samples. After further synthesis of HAP@CRH, the surface presented a honeycomb-like structure as its porosity increased. The BET specific surface area increased from 1.06 m^2/g (RH) to 193.64 m^2/g (CRH) and 183.91 m^2/g (HAP@CRH) respectively, while the total pore volume increased from almost zero to 0.089 and 0.202 cm^3/g, respectively.

The CRH showed a remarkably higher adsorption effect on the Cr(VI) ions than that of RH, and the adsorption property was further enhanced as CRH modified to be HAP@CRH after depositing hydroxyapatite particles onto the surfaces of CRH. The Cr(VI) ions solution with an initial concentration of 30 mg/L was treated with adsorbent dosages of 5.0 g/L at 30°C, pH = 2.0, within a contact time of 24 h. The residual concentration and removal rate of Cr(VI) ions were determined as 0.43 mg/L and 98.57% respectively.

Acknowledgements

This work was financially supported by Jiangxi Provincial Natural Science Foundation (20212BAB214012). Thanks are also due to "the Scientific and Technological Research Project of Education Department in Jiangxi Province" (Grant No. GJJ190340) and the Postdoctoral merit-based fund Research Projects of Jiangxi Province Human Resources and Social Security Department (Grant No. 2020KY38).

References

[1] X. Xiao, B.L. Chen, Z.M. Chen, L.Z. Zhu, L.S. Jerald, Insight into multiple and multilevel structures of biochars and their potential environmental applications: a critical review, Environ. Sci. Technol., 52 (2018) 5027–5047.
[2] A. Saravanan, P. Senthil Kumar, D.-V.N. Vo, S. Swetha, P. Tsopbou Ngueagni, S. Karishma, S. Jeevanantham, P.R. Yaashikaa, Ultrasonic assisted agro waste biomass for rapid removal of Cd(II) ions from aquatic environment: mechanism and modelling analysis, Chemosphere, 271 (2021) 129484, doi: 10.1016/j.chemosphere.2020.129484.
[3] A. Uihlein, L. Schebek, Environmental impacts of a lignocellulose feedstock biorefinery system: an assessment, Biomass Bioenergy, 33 (2009) 793–802.
[4] A.N. Swami Nathen, R.S. Robert, Indian rice husk ash – improving the mechanical properties of concrete: a review, Int. J. Eng. Res. Appl., 7 (2017) 76–79.
[5] N. Shukla, D. Sahoo, N. Remya, Biochar from microwave pyrolysis of rice husk for tertiary wastewater treatment and soil nourishment, J. Cleaner Prod., 235 (2019) 1073–1079.
[6] J. Acharya, U. Kumar, P. Mahammed Rafi, Removal of heavy metal ions from wastewater by chemically modified agricultural waste material as potential adsorbent-a review, Int. J. Curr. Eng. Technol., 8 (2018) 526–530.
[7] V.R. Madduluri, K.K. Mandari, V. Velpula, M. Varkolu, S.R.R. Kamaraju, M. Kang, Rice husk-derived carbon-silica supported Ni catalysts for selective hydrogenation of biomass-derived furfural and levulinic acid, Fuel, 261 (2020) 116339, doi: 10.1016/j.fuel.2019.116339.
[8] D. An, Y. Guo, Y. Zhu, Z. Wang, A green route to preparation of silica powders with rice husk ash and waste gas, Chem. Eng. J., 162 (2010) 509–514.
[9] H. Basu, S. Saha, I.A. Mahadevan, M.V. Pimple, R.K. Singhal, Humic acid coated cellulose derived from rice husk: a novel biosorbent for the removal of Ni and Cr, J. Water Process Eng., 32 (2019) 100892, doi: 10.1016/j.jwpe.2019.100892.
[10] P. Chen, W. Gu, W. Fang, X. Ji, R. Bie, Removal of metal impurities in rice husk and characterization of rice husk ash under simplified acid pretreatment process, Environ. Prog. Sustainable Energy, 36 (2017) 830–837.
[11] S. Handley-Sidhu, J.C. Renshaw, S. Moriyama, B. Stolpe, C. Mennan, S. Bagheriasl, P. Yong, A. Stamboulis, M. Paterson-Beedle, K. Sasaki, R.A.D. Pattrick, J.R. Lead, L.E. Macaskie, Uptake of Sr^{2+} and Co^{2+} into biogenic hydroxyapatite: implications for biomineral ion exchange synthesis, Environ. Sci. Technol., 45 (2011) 6985–6990.
[12] Z.P. Yang, C.J. Zhang, Adsorption/desorption behavior of protein on nanosized hydroxyapatite coatings: a quartz crystal microbalance study, Appl. Surf. Sci., 255 (2009) 4569–4574.
[13] Z. Zhu, L. Li, H. Zhang, Y. Qiu, J. Zhao, Adsorption of lead and cadmium on Ca-deficient hydroxyapatite, Sep. Sci. Technol., 45 (2010) 262–268.
[14] W. Xiong, Y. Yang, D. Huang, L. Hu, J. Wang, C. Zhang, L. Jiang, M. Cheng, C. Zhou, M. Chen, G. Zeng, C. Lai, Semiconductor/boron nitride composites: synthesis, properties, and photocatalysis applications, Appl. Catal., B, 238 (2018) 6–18.
[15] L. Yuan, M. Yan, Z. Huang, K. He, G. Zeng, A. Cheng, L. Hu, H. Li, M. Peng, T. Huang, Influences of pH and metal ions on the interactions of oxytetracycline onto nano-hydroxyapatite and their co-adsorption behavior in aqueous solution, J. Colloid Interface Sci., 541 (2019) 101–113.
[16] S. Saoiabi, A. Gouza, H. Bouyarmane, A. Laghzizil, A. Saoiabi, Organophosphonate-modified hydroxyapatites for Zn(II) and Pb(II) adsorption in relation of their structure and surface properties, J. Environ. Chem. Eng., 4 (2015) 428–433.
[17] W. Liu, S. Tian, X. Zhao, W. Xie, Y. Gong, D. Zhao, Application of stabilized nanoparticles for in situ remediation of metal-contaminated soil and groundwater: a critical review, Curr. Pollut. Rep., 1 (2015) 280–291.
[18] S. Mignardi, A. Corami, V. Ferrini, Evaluation of the effectiveness of phosphate treatment for the remediation of mine waste soils contaminated with Cd, Cu, Pb, and Zn, Chemosphere, 86 (2012) 354–360.
[19] X. Peng, J. Wu, Z. Zhao, X. Wang, H. Dai, L. Xu, G. Xu, Y. Jian, F. Hu, Activation of peroxymonosulfate by single-atom Fe-g-C_3N_4 catalysts for high efficiency degradation of tetracycline via nonradical pathways: role of high-valent iron-oxo species and Fe–N_x sites, Chem. Eng. J., 427 (2022) 130803, doi: 10.1016/j.cej.2021.130803.
[20] M. Iqbal, M. Abbas, J. Nisar, A. Nazir, Bioassays based on higher plants as excellent dosimeters for ecotoxicity monitoring: a review, Chem. Int., 5 (2019) 1–80.
[21] M. Abbas, M. Adil, S. Ehtisham-ul-Haque, B. Munir, M. Yameen, A. Ghaffar, G.A. Shar, M.A. Tahir, M. Iqbal, *Vibrio fischeri* bioluminescence inhibition assay for ecotoxicity assessment: a review, Sci. Total. Environ., 626 (2018) 1295–1309.

[22] H. Rasoulzadeh, A. Sheikhmohammadi, M. Abtahi, B. Roshan, R. Jokar, Eco-friendly rapid removal of palladium from aqueous solutions using alginate-diatomite magnano composite, J. Environ. Chem. Eng., 9 (2021) 105954, doi: 10.1016/j.jece.2021.105954.
[23] H. Godini, F. Hashemi, L. Mansuri, M. Sardar, G. Hassani, S.M. Mohseni, A.A. Alinejad, S. Golmohammadi, A.S. Mohammadi, Water polishing of phenol by walnut green hull as adsorbent: an insight of adsorption isotherm and kinetic, J. Water Reuse Desal., 6 (2016) 544–552.
[24] A. Kausar, H.N. Bhatti, M. Iqbal, A. Ashraf, Batch versus column modes for the adsorption of radioactive metal onto rice husk waste: conditions optimization through response surface methodology, Water Sci. Technol., 76 (2017) 1035–1043.
[25] Y.Y. Wang, Y.X. Liu, H.H. Lu, R.Q. Yang, S.M. Yang, Competitive adsorption of Pb(II), Cu(II), and Zn(II) ions onto hydroxyapatite-biochar nanocomposite in aqueous solutions, J. Solid State Chem., 261 (2018) 53–61.
[26] Y.C. Long, J. Jiang, J. Hu, X.J. Hu, Q. Yang, S.Q. Zhou, Removal of Pb(II) from aqueous solution by hydroxyapatite/carbon composite: preparation and adsorption behavior, Colloids Surf., A, 577 (2019) 471–479.
[27] M.M. Wang, K.M. Zhang, M.Y. Wu, Q.Y. Wu, J.Y. Liu, J.J. Yang, J.N. Zhang, Unexpectedly high adsorption capacity of esterified hydroxyapatite for heavy metal removal, Langmuir, 35 (2019) 16111–16119.
[28] Z. Chen, B. Chen, C.T. Chiou, Fast and slow rates of naphthalene sorption to biochars produced at different temperatures, Environ. Sci. Technol., 46 (2016) 11104–11111.
[29] N. Alias, N. Ibrahim, M. Hamid, H. Hasbullah, R.R. Ali, A.N. Sadikin, U.A. Asli, Thermogravimetric analysis of rice husk and coconut pulp for potential biofuel production by flash pyrolysis, Malays. J. Anal. Sci., 18 (2014) 705–710.
[30] B. Chen, Z. Chen, Sorption of naphthalene and 1-naphthol by biochars of orange peels with different pyrolytic temperatures, Chemosphere, 76 (2009) 127–133.
[31] H. Yang, Y. Rong, H. Chen, D.H. Lee, C. Zheng, Characteristics of hemicellulose, cellulose and lignin pyrolysis, Fuel, 86 (2007) 1781–1788.
[32] K. Yadav, M. Tyagi, S. Kumari, S. Jagadevan, Influence of process parameters on optimization of biochar fuel characteristics derived from rice husk: a promising alternative solid fuel, Bioenergy Res., 12 (2019) 1052–1065.
[33] L. Lian, X. Cao, Y. Wu, D. Sun, D. Lou, A green synthesis of magnetic bentonite material and its application for removal of microcystin-LR in water, Appl. Surf. Sci., 289 (2014) 245–251.
[34] W.B. Guan, B.X. Zhao, S. Qiu, N. Liu, N. Lu, R. Cheng, Y. Sun, The adsorption behavior of Cr(VI) on modified montmorillonite, J. Northwest Univ., 46 (2016) 375–380.
[35] J. Yi, Z. Huo, A.M. Asiri, K.A. Alamry, J. Li, Application of agroforestry waste biomass adsorption materials in water pollution treatment, J. Prog. Chem., 31 (2019) 760–762 (in Chinese).
[36] T.K. Sen, D. Gomez, Adsorption of zinc (Zn^{2+}) from aqueous solution on natural bentonite, Desalination, 267 (2011) 286–294.
[37] M.S. Fernando, R.M.D. Silva, K.M.N.D. Silva, Synthesis, characterization, and application of nano hydroxyapatite and nanocomposite of hydroxyapatite with granular activated carbon for the removal of Pb^{2+} from aqueous solutions, Appl. Surf. Sci., 351 (2015) 95–103.
[38] Y. Zhang, Z. Ma, Q. Zhang, J. Wang, Q. Ma, Y. Yang, X. Luo, W. Zhang, Comparison of the physicochemical characteristics of bio-char pyrolyzed from moso bamboo and rice husk with different pyrolysis temperatures, Bioresources, 12 (2017) 4652–4669.
[39] Z. Shen, Y. Zhang, O. Mcmillan, F. Jin, A. Al-Tabbaa, Characteristics and mechanisms of nickel adsorption on biochars produced from wheat straw pellets and rice husk, Environ. Sci. Pollut. Res. Int., 24 (2017) 12809–12819.
[40] C. Subrahmanyam, D.A. Bulushev, L. Kiwi-Minsker, Dynamic behavior of activated carbon catalysts during ozone decomposition at room temperature, Appl. Catal., B, 61 (2005) 98–106.
[41] M.P. da Rosa, A.V. Igansi, S.F. Lütke, T.R.S.C. Junior, A.C.R. do Santos, A.P. de Oliveira Lopes Inacio, L.A. de Almeida Pinto, P.H. Beck, A new approach to convert rice husk waste in a quick and efficient adsorbent to remove cationic dye from water, J. Environ. Chem. Eng., 7 (2019) 103504, doi: 10.1016/j.jece.2019.103504.
[42] P. Kaur, P. Kaur, K. Kaur, Adsorptive removal of imazethapyr and imazamox from aqueous solution using modified rice husk, J. Cleaner Prod., 244 (2019) 118699, doi: 10.1016/j.jclepro.2019.118699.
[43] X. Li, Q. Shen, D. Zhang, X. Mei, R. Wei, Y. Xu, G. Yu, M. Andrea, Functional groups determine biochar properties (pH and EC) as studied by two-dimensional ^{13}C NMR correlation spectroscopy, PLoS One, 8 (2013) e65949, doi: 10.1371/journal.pone.0065949.
[44] G.S. Kumar, G. Karunakaran, E.K. Girija, E. Kolesnikov, N.V. Minh, M.V. Gorshenkov, D. Kuznetso, Size and morphology-controlled synthesis of mesoporous hydroxyapatite nanocrystals by microwave-assisted hydrothermal method, Ceram. Int., 44 (2018) 11257–11264.
[45] D. MubarakAli, Microwave irradiation mediated synthesis of needle-shaped hydroxyapatite nanoparticles as a flocculant for *Chlorella vulgaris*, Biocatal. Agric. Biotechnol., 17 (2019) 203–206.
[46] H. Nishida, M. Kimata, T. Ogata, T. Kawei, Malodors adsorption behavior of metal cation incorporated hydroxyapatite, J. Environ. Chem. Eng., 5 (2017) 52815–2819.
[47] Z. Li, X. Liu, Y. Wang, Modification of sludge-based biochar and its application to phosphorus adsorption from aqueous solution, J. Mater. Cycles Waste Manage., 22 (2020) 123–132.
[48] M. Li, S. Ma, X. Zhu, Preparation of activated carbon from pyrolyzed rice husk by leaching out ash content after CO_2 activation, Bioresources, 11 (2016) 3384–3396.
[49] D.L. Yao, B.S. Jin, H. Tao, Experimental study on thermogravimetry-FTIR of rice husk, Energy Res. Util., 3 (2008) 11–15 (in Chinese).
[50] Y. Shen, K. Yoshikawa, Tar conversion and vapor upgrading via in situ catalysis using silica-based nickel nanoparticles embedded in rice husk char for biomass pyrolysis/gasification, Ind. Eng. Chem. Res., 53 (2014) 10929–10942.
[51] D. Wang, L. Chu, M. Paradelo, W.J.G.M. Peijnenburg, Y. Wang, D. Zhou, Transport behavior of humic acid-modified nano-hydroxyapatite in saturated packed column: effects of Cu, ionic strength, and ionic composition, J. Colloid Interface Sci., 360 (2011) 398–407.
[52] Ö. Akçakal, M. Şahin, M. Erdem, Synthesis and characterization of high-quality activated carbons from hard-shelled agricultural wastes mixture by zinc chloride activation, Chem. Eng. Commun., 206 (2018) 888–897.
[53] K. Legrouri, E. Khouya, H. Hannache, M. El Hartti, M. Ezzine, R. Naslain, Activated carbon from molasses efficiency for Cr(VI), Pb(II) and Cu(II) adsorption: a mechanistic study, Chem. Int., 3 (2017) 301–310.
[54] M. Kapnisti, F. Noli, P. Misaelides, G. Vourlias, D. Karfaridis, A. Hatzidimitriou, Enhanced sorption capacities for lead and uranium using titanium phosphates; adsorption, kinetics, equilibrium studies and mechanism implication, Chem. Eng. J., 342 (2018) 184–195.
[55] B.M. Weckhuysen, I.E. Wachs, R.A. Schoonheydt, Surface chemistry and spectroscopy of chromium in inorganic oxides, Chem. Rev., 96 (1996) 3327–3350.
[56] C. Zou, J. Liang, J. Wei, Y. Guan, Y. Zhang, Adsorption behavior of magnetic bentonite for removing Hg(II) from aqueous solutions, RSC Adv., 8 (2018) 27587–27595.
[57] C. Zou, W. Jiang, J. Liang, X. Sun, Y. Guan, Removal of Pb(II) from aqueous solutions by adsorption on magnetic bentonite, Environ. Sci. Pollut. Res., 26 (2019) 1315–1322.
[58] Y. Feng, J.L. Gong, G.M. Zeng, Q.Y. Niu, H.Y. Zhang, C.G. Niu, J.H. Deng, M. Yan, Adsorption of Cd(II) and Zn(II) from aqueous solutions using magnetic hydroxyapatite nanoparticles as adsorbents, Chem. Eng. J., 162 (2010) 487–494.
[59] M. Su, D.C.W. Tsang, X. Ren, Q. Shi, J. Tang, H. Zhang, L. Kong, L. Hou, G. Song, D. Chen, Removal of U(VI) from nuclear mining effluent by porous hydroxyapatite: evaluation on

characteristics, mechanisms and performance, Environ. Pollut., 254 (2019) 112891, doi: 10.1016/j.envpol.2019.07.059.
[60] M. Akram, H.N. Bhatti, M. Iqbal, S. Noreen, S. Sadaf, Biocomposite efficiency for Cr(VI) adsorption: kinetic, equilibrium and thermodynamics studies, J. Environ. Chem. Eng., 5 (2016) 400–411.
[61] G. Bharath, D. Prabhu, D. Mangalaraj, C. Viswanathan, N. Ponpandian, Facile in-situ growth of Fe_3O_4 nanoparticles on hydroxyapatite nanorods for pH dependent adsorption and controlled release of proteins, RSC Adv., 4 (2014) 50510–50520.
[62] I.A. Bhatti, N. Ahmad, N. Iqbal, M. Zahid, M. Iqbal, Chromium adsorption using waste tire and conditions optimization by response surface methodology, J. Environ. Chem. Eng., 5 (2017) 2740–2751.

Supplementary information

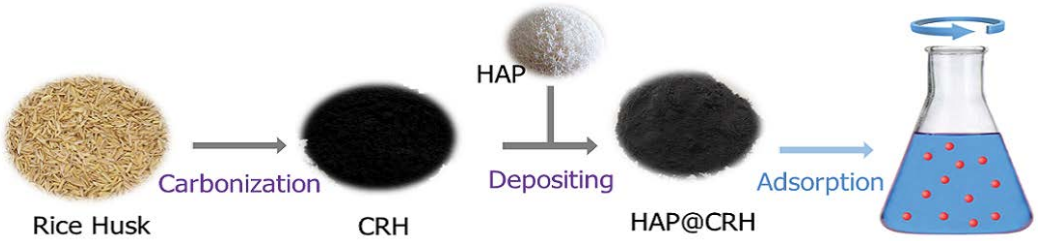

Fig. S1. Schematic representation of the preparation procedures of HAP@CRH.

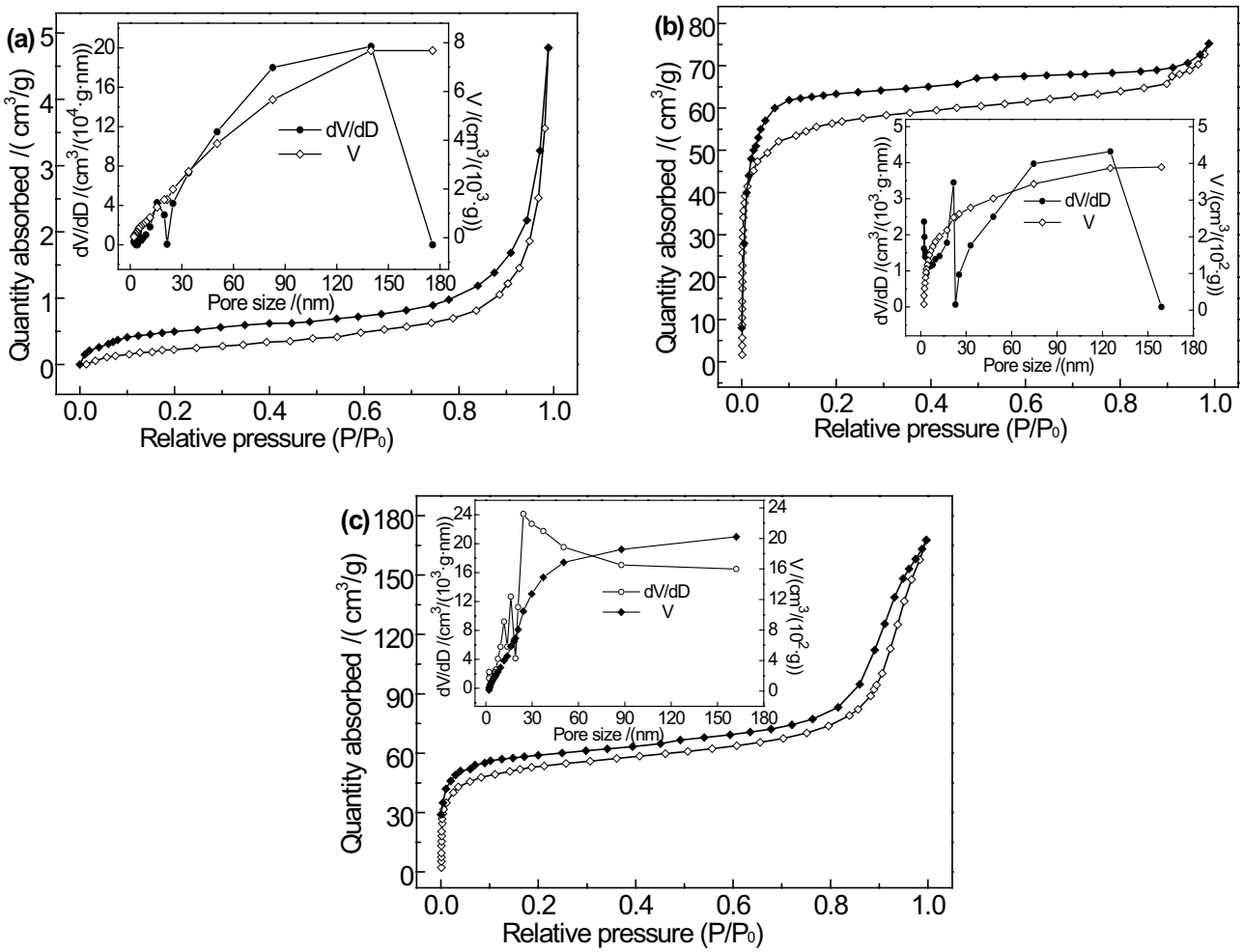

Fig. S2. N_2 adsorption–desorption isotherms and pore-size distributions of (a) RH, (b) CRH and (c) HAP@CRH samples.

Table S1
Comparison of adsorption properties for Cr(VI) ions with several modified rice husk materials

Samples	Dose of adsorbent	Initial Cr(VI) concentration	Adsorbed capacity	Removal rate	Modification method	Reference
Rice husk	5 g/L	40 mg/L	1.58 mg/g (experiment)	19.75%	Unmodified	This Study
Carbonized rice husk	5 g/L	40 mg/L	7.36 mg/g (experiment)	92.03%	Carbonizing RH at 600°C for 2.0 h	
Hydroxyapatite-modified carbonized rice husk	5 g/L	40 mg/L	7.91 mg/g (experiment)	98.70%	Depositing hydroxyapatite particles on the surface of CRH with a Ca^{2+}/CRH ratio of 0.2 g/g	
Parboiled-rice husk ash (RHA)	5 g/L	45 mg/L	3.29 mg/g (experiment)	35.6%	The $RHAH^+$ was prepared through the parboiled-rice husk ash was subjected to acid treatment using H_2SO_4 (1% v/v)	[S1]
Parboiled-rice husk ash modified by sulfur acid ($RHAH^+$)			8.83 mg/g (experiment)	98.1%		
Rice husk	20 g/L	5.0 mg/L	0.235 mg/g (experiment)	94.0%	Modification method is not clear as only the abstract of this document was retrieved, but the whole article could not be retrieved	[S2]
Rice husk ash			0.221 mg/g (experiment)	88.4%		
Rice husk	20 g/L	–	3.78 mg/g (Langmuir)	–		
Rice husk ash			2.27 mg/g (Langmuir)	–		
Carbonized acid-treated rice husk (CRH)	10 g/L	10 mg/L	0.49 mg/g (experiment)	49%	Rice husk was treated with 5 M HNO_3 solution, HNO_3-treated rice wash was carbonized in a tubular furnace at 700°C for 5 h under a N_2 flow. CRH was then treated with different concentrations of NaOH	[S3]
CRH1M			0.56 mg/g (experiment)	56%		
CRH3M			0.67 mg/g (experiment)	67%		
CRH5M			0.86 mg/g (experiment)	86%		
Ozone treated rice husk carbon	4.0 g/L	50 mg/L	11.88 mg/g (experiment)	95%	Rice husk was carbonized at 800°C under N_2 flow for 160 min, then it was reacted with ozone (1,100 mg/L) for 3 h	[S4]
	4.0 g/L	–	62.9 mg/g (Langmuir)	–		
Black rice husk ash (BRHA)	15.0 g/L	100 mg/L	5.559 mg/g (Kinetic)	83.39%	Pyrolysis of raw rice husks under nitrogen atmosphere	[S5]
	15.0 g/L	50 mg/L	2.931 mg/g (Kinetic)	87.93%		
Pre-boiled rice husk (BRH)			6.31 mg/g (experiment)	50.48%	It was boiled with distilled water for 5 h	
Formaldehyde treated rice husk (FRH)	4 g/L	50 mg/L	7.67 mg/g (experiment)	61.36%	Rice husk was treated with 1% formaldehyde in the ratio of 1:5 (rice husk: formaldehyde, w/v) at room temperature (27°C ± 3°C) for 24 h	[S6]

References

[S1] V.S. Gamboa, E.V. Benvenutti, É.J. Kinast, M. Pires, F.P. Gasparin, L.A. da Silva Ries, Efficient removal of chromium(VI) from dilute aqueous solutions using agro-industrial residue based on parboiled-rice husk ash, Chem. Eng. Commun., 209 (2022) 1096–1110.

[S2] G.C. Ghosh, S. Zaman, T.K. Chakraborty, Adsorptive removal of Cr(VI) from aqueous solution using rice husk and rice husk ash, Desal. Water Treat., 130 (2018) 151–160.

[S3] B.D. Mukri, K. Krushnamurty, A. Chowdhury, D. Suryakala, C. Subrahmanyam, Alkali-treated carbonized rice husk for the removal of aqueous Cr(VI), BioResources, 11 (2016) 9175–9189.

[S4] S. Sugashini, K.M.M.S. Begum, Preparation of activated carbon from carbonized rice husk by ozone activation for Cr(VI) removal, New Carbon Mater., 30 (2015) 252–261.

[S5] V.G. Georgieva, M.P. Tavlieva, S.D. Genieva, L.T. Vlaev, Adsorption kinetics of Cr(VI) ions from aqueous solutions onto black rice husk ash, J. Mol. Liq., 208 (2015) 219–226.

[S6] M. Bansal, U. Garg, D. Singh, V.K. Garg, Removal of Cr(VI) from aqueous solutions using pre-consumer processing agricultural waste: a case study of rice husk, J. Hazard. Mater., 162 (2009) 312–320.